Available online at www.sciencedirect.com
ScienceDirect
International Journal of Heat and Mass Transfer 50 (2007) 2772–2786
International Journal of HEAT and MASS TRANSFER
www.elsevier.com/locate/ijhmt

Experimental investigation on natural convection in a convergent channel with uniformly heated plates

Nicola Bianco [a], Oronzio Manca [b,*], Sergio Nardini [b]

[a] Dipartimento di Energetica, Termofluidodinamica applicata e Condizionamenti ambientali, Università degli Studi di Napoli Federico II, Piazzale Tecchio 80, 80125, Napoli, Italy

[b] Dipartimento di Ingegneria Aerospaziale e Meccanica, Seconda Università degli Studi di Napoli, Via Roma 29, 81031, Aversa (CE), Italy

Received 21 July 2006
Available online 16 January 2007

Abstract

An experimental investigation on natural convection in air in vertical convergent channels with wall uniform heat flux is presented. Wall temperatures show that by increasing the spacing the effect of the convergence angle decreases. For the lowest spacing, a significant decrease of maximum wall temperature occurs passing from the parallel vertical plate configurations to convergence angles $\theta \geqslant 2^\circ$.

Dimensionless wall maximum temperature and Nusselt numbers are evaluated and correlated to the Rayleigh number or the channel Rayleigh number. The correlations are in the ranges $2.85 \leqslant Ra'_{bmin} \leqslant 1.22 \times 10^5$ and $0^\circ \leqslant \theta \leqslant 10^\circ$.

Flow visualization is carried out both numerically and experimentally. Numerical and experimental data are compared and a good agreement has been found.

1. Introduction

The thermal control of many systems, such as electronics, often requires an accurate prediction of the performance of natural convection in channels [1,2]. As far as cooling of electronic equipment is concerned, an interesting problem is the heat transfer in a convergent channel with two uniformly heated flat plates [3–13]. The determination of the thermal performance of these configurations is rather difficult because of the large number of thermal and geometric variables. Experimental and numerical investigations can therefore give useful information on the effects of the heat flux, the inclination angle and the spacing.

Natural convection in channels has been widely investigated both numerically [2] and experimentally [14] for different boundary conditions at the principal walls of the channel. The present research efforts are devoted to define those channel configurations that can improve its thermal performance [15]. Among them a very simple configuration is the convergent vertical channel with two principal parallel walls [3–13,16]. The first numerical and experimental study of water natural convection in a convergent vertical channel was carried out by Sparrow et al. [3]. The principal converging walls were maintained at the same uniform temperature and the angles from the vertical varied between 0° and 15°. The authors found that the Nusselt numbers for the convergent channels could be brought into very close agreement with those for the parallel-walled channel by employing correlation variables based on the maximum interwall spacing as the characteristic dimension. The study was extended to the diverging channels by Sparrow and Ruiz [4]. They found that the correlation for vertical channels with parallel walls could be adapted to converging and diverging channels, by using the maximum interwall spacing. Kihm et al. [16] experimentally investigated air natural convection in a uniform wall temperature converging channel using a specklegram technique. Local and average heat transfer coefficients were

* Corresponding author. Tel.: +39 0815010217; fax: +39 0815010204.
E-mail address: oronzio.manca@unina2.it (O. Manca).

0017-9310/$ - see front matter © 2006 Elsevier Ltd. All rights reserved.
doi:10.1016/j.ijheatmasstransfer.2006.11.017

Nomenclature

a	thermal diffusivity, $m^2\,s^{-1}$
b	channel spacing (b_{min} or b_{av} or b_{max}), m
g	acceleration of gravity, $m\,s^{-2}$
Gr	channel Grashof number, Eq. (1)
k	thermal conductivity, $W\,m^{-1}\,K^{-1}$
L	channel length, m
Nu	Nusselt number, Eq. (3)
p	pressure, Pa
Pr	Prandtl number
q	heat flux, W/m^2
r	regression coefficient
R	dependent variable, Eq. (7)
Ra	Rayleigh number, Eq. (1)
Ra'	$Ra\,(b/L)$, channel Rayleigh number
T	temperature, K
T^+	dimensionless temperature, Eq. (5)
u, v	velocity components, $m\,s^{-1}$
W	channel width, m
x, y	coordinates along the plate, m
X_i	independent variable, Eq. (7)

Greek symbols

β	volumetric coefficient of expansion, K^{-1}
θ	inclination angle, °
ν	kinematic viscosity, $m^2\,s^{-1}$
ρ	density, $kg\,m^{-3}$

Subscripts

av	average
b	channel spacing (bmin or bav or bmax)
bav	average channel spacing
bmax	maximum channel spacing
bmin	minimum channel spacing
c	convective
f	fluid
k	conductive
min	minimum
max	maximum
o	ambient air
r	radiative
s	solid
w	wall
Ω	Ohmic dissipation

evaluated for five inclination angles (0–60°) and eight channel exit openings. Haung et al. [11] accomplished an experimental study of mixed convection in a vertical convergent channel. The channel was heated asymmetrically at uniform heat flux. The heated wall was vertical and the opposite wall was insulated and convergent with an angle of 3°. Flow visualization was employed in order to visualize the flow structure. Local and average Nusselt numbers were evaluated and correlated in terms of relevant dimensionless parameters.

Natural convection in air in uniform wall temperature converging vertical channels was studied numerically by Said [5]. The best correlation for the Nusselt number at low Rayleigh numbers ($<10^2$) was achieved by the use of the maximum channel spacing as the characteristic dimension. Shalash et al. [6] investigated numerically and experimentally, the same configuration studied in [5]. The computational domain was extended upstream and downstream of the channel. A Mach-Zender interferometer was used to perform the experiments. The authors found that, at low Rayleigh numbers, increasing the angle significantly increases the Nusselt number, whereas, at high Rayleigh numbers, increasing the angle, the Nusselt number decreases. When the inclination angle was increased, the local Nusselt number decreased near the channel inlet and increased near the channel outlet, particularly at low Rayleigh numbers. A two-dimensional numerical simulation of natural convection in a converging channel was accomplished in [7]. The influence of converging angle on local and average Nusselt numbers was studied. A blended correlation for average Nusselt number in isothermal channels was proposed in the Rayleigh number range $1–10^6$ and convergence angle range 0–30°. Results for asymmetric heating conditions were also given and, for these configurations, a region of downflow and recirculation appeared at the channel outlet zone for high Rayleigh number. This effect tended to diminish when converging angle increased. A numerical investigation on natural convection in air in vertical diverging and converging channels was carried out in [8]. A nonuniform wall heating was considered and it was modelled as an isothermal zone with its length lower or equal to the wall length. The adiabatic zone was placed either at the bottom end of the channel or at the top end. The Rayleigh number was based on the wall length and the numerical simulations were obtained in the Rayleigh number range between 10^5 and 10^6. The results showed that the optimal angle between the two walls was approximately zero when the Rayleigh number was large. Natural convection in air in a convergent channel with the two principal flat plates at uniform heat flux, with finite thickness and thermal conductivity, was numerically studied in [9]. An extended computational domain was adopted. Temperature profiles were strongly affected by the convergence angle at low Rayleigh numbers, whereas the opposite occured at high Rayleigh numbers. At the lower minimum gap, streamlines and isotherms highlighted a low pressure zone

in the channel, due to a choked flow in its upper region. Marcondes et al. [12] carried out a numerical investigation on natural convection in parallel, convergent and divergent channels using a fully elliptic procedure considering only the simple channel as computational domain. Both the channel walls were at uniform temperature and results were given for Prandtl number ranging from 0.7 to 88. A correlation for average Nusselt number, Rayleigh number, in terms of maximum channel width and channel aspect ratio, and Prandtl number was proposed. They found that for convergent channels a recirculation region in the outlet zone was observed. Design charts for the evaluation of thermal and geometrical parameters of vertical convergent channels were presented by Bianco et al. [13]. Correlations for dimensionless maximum wall temperature and average Nusselt number, in terms of Rayleigh numbers and geometrical parameters, for natural convection in air, in a vertical convergent channel, with symmetrically heated walls, were proposed. The results were obtained elaborating the numerical data carried out in [9,10]. A simple procedure to evaluate the optimal geometrical configurations in terms of channel spacing and convergence angle was presented.

In the authors' opinion, there is a lack of experimental data on natural convection in air ($Pr = 0.71$) in vertical convergent channels with uniform heat flux at the principal walls as shown in Table 1. Therefore, an experimental investigation has been carried out. In this paper, results in terms of wall temperature profiles are presented as a function of the walls inclination angle, the distance between the walls and the heat flux. The experimental results are compared with the ones carried out with the numerical model given in [9,13]. Therefore, the present paper allows to verify experimentally the results and conclusions reported in [9,13]. The comparison is accomplished in terms of stream function fields obtained numerically and visualization obtained experimentally. Nusselt numbers and dimensionless maximum wall temperatures are evaluated and correlated to the channel Rayleigh numbers and dimensionless geometrical parameters.

2. Experimental apparatus

The investigated test section is shown in Fig. 1, where x and y are the coordinates along the length and the width of the plate, respectively. The channel is made of two principal plates, symmetrically heated at uniform heat flux and two unheated plexiglass side walls (Fig. 1a). It is open to the ambient along the top and the bottom edges.

The cross-section of the isoflux principal walls of the channel is sketched in Fig. 1b. Each wall was made with a 3.2 mm thick, 406 mm long and 530 mm wide phenolic fiberboard plate, with a typical thermal conductivity of 0.17 W m^{-1} K^{-1}. Its surface facing the channel was coated with a 16 μm thick copper layer, which was the heater. It was obtained by cutting the copper in a 2.5 mm wide and 38 m long serpentine track and its expected electric resistance was about 8.0 Ω. A thick copper bar, bolted to

Table 1
Comparison among different studies of natural convection in convergent channels

Reference	Type of investigation	Boundary conditions on channel walls	Conduction on walls	Radiative effect	δ	Reference length	L/b	Ra'	Correlation
Sparrow et al. (1988) [3]	Numerical and experimental	UWT	None	None	0°, 2°, 5°, 10°, 15°	b_{max}	11.4, 22.9	4×10^3–7×10^4	Yes
Kihm et al. (1993) [16]	Numerical and experimental	UWT	None	None	0°, 15°, 30°, 45°, 60°	b_{min}	2.5–14	1–1×10^8	None
Said (1996) [5]	Numerical and experimental	UWT	None	None	0°, 2°, 5°, 10°	b_{max}	–	1–2×10^4	None
Shalash et al. (1997) [6]	Numerical and experimental	UWT	None	None	0°, 2°, 4°, 8°	$b_{min}/2$	6, 8.5, 12	6.4–4.8×10^4	Yes
Kaiser et al. (2004) [7]	Numerical	UWT	None	None	0–60°	b_{min}	0.5–50	1–110^6	Yes
Bejan et al. (2004) [8]	Numerical	UWT	None	None	0–5°	L_w	–	1×10^5–1×10^7	None
Bianco and Nardini (2005) [9]	Numerical	UWHF	Yes	None	0°, 2°, 5°, 10°	b_{max}	12–58	4.4–2.9×10^8	Yes
Bianco et al. (2006) [10]	Numerical and experimental	UWHF	Yes	Yes	0°, 2°, 5°, 10°	b_{min}	10–58	4.4–1.5×10^5	Yes
Marcondes et al. (2006) [12]	Numerical	UWT	None	None	0°, 5°, 15°	b_{max}	1.65, 3.82, 11.4	1×10^5–1×10^8	Yes
Bianco et al. (2006) [13]	Numerical	UWHF	Yes	Yes	0–10°	b_{max}	2.0–60	4.6–1.8×10^8	Yes
Present work	Experimental and numerical	UWHF	Yes	None	0°, 2°, 5°, 10°	b_{min}	10–58	2.85–1.22×10^5	Yes

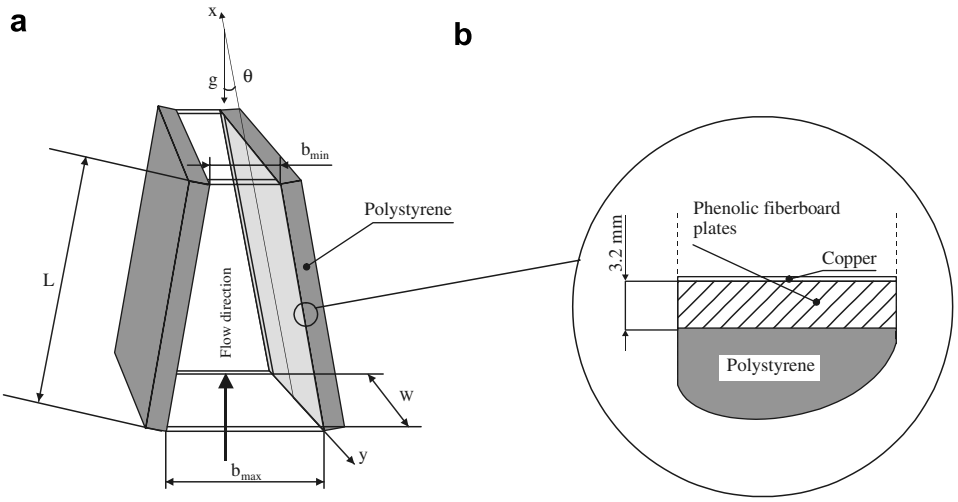

Fig. 1. (a) Sketch of the test section; (b) particular of the heated walls.

the electric supply wire, was soldered to the ends of each heater. The dissipated heat flux was evaluated with an accuracy of ±2%, by measuring the voltage drop and the current through the electric resistance. A maximum variation of ±10% in the electrical resistivity of the copper was evaluated in the worst conditions, when the maximum difference in the wall temperatures was 30 K. Therefore, a uniform wall heat flux was assumed, with a ±5% maximum deviation from its average value. Heat losses from the back of the heated walls were reduced by sticking a 150 mm polystyrene block on the rear surface of each wall. The total normal emissivity of the walls was 0.1 and was obtained by sticking a self-adhesive 25 μm thick aluminum foil on the surfaces facing the channel. The emissivity was evaluated by means of radiometric direct measurements. The electric insulation between the copper surfaces and the aluminum foil was assured by uniformly spraying an electrically insulating varnish onto them before coating. Side walls were two trapezoidal plexiglass plates, 4.0 mm thick, placed between the principal walls at their lateral edges. They were machined within an accuracy of ±0.03 mm. The distance between the principal walls was measured with an accuracy of ±0.25 mm using a dial-gauge caliper which can resolve ±0.025 mm. The inclination angle was set and verified by measuring the maximum and the minimum spacings. The walls were fastened together by a steel frame, which was designed in such a way as not to obstruct the fluid flow in the proximity of the channel inlet. A hinge at the top of the principal walls allowed their rotation in order to obtain a convergent channel. The channel was aligned vertically, with horizontal leading edges, by means of a plumb line and a level. The entire apparatus was located in an enclosed room, accurately sealed in order to eliminate extraneous air currents and air drafts were further reduced by vertical screens, 2.5 m high. A large fraction of the lower part of the screens was made up of a 0.20 m high mesh. The range of ambient temperature varied from 21 to 22 °C during the experiments; the measured differences in the air ambient temperature in the proximity of the inlet and the exit sections of the apparatus were less than 0.8 K.

The principal walls of the channel were 406 mm long and 450 mm wide. The values of the minimum channel gap were $b_{\min} = 7.0$ mm, 10.0 mm, 20.0 mm, 32.3 mm and 40.0 mm. The convergence angle, θ, varied in the 0–10° range; consequently, the maximum channel spacing, $b_{\max}$, varied in the 7.0–148.0 mm range when $b_{\min}$ was 7.0 mm and in the 40.0–181.0 mm range when $b_{\min}$ was 40.0 mm.

Wall temperature measurements were carried out by 0.50 mm OD iron-constantan (type J) thermocouples, embedded in the fiberboard in the very proximity of the back side of the copper layer and bonded with a 3 M epoxy glue. They were run horizontally, parallel to the surfaces, thereby lying along isotherms in order to minimize conduction heat losses in the leads. Sixteen thermocouples were placed in the centerline of each plate at the following locations: $x = 2.5, 12.7, 38.1, 73.7, 88.9, 104.1, 124.5, 139.7, 154.9, 175.3, 190.5, 205.7, 241.3, 281.9, 342.9, 403.9$ mm.

At 300 mm from the leading edge of one of the walls, eight additional thermocouples were horizontally located outward from the centerline at $y = \pm 75.0$ mm, ±100.0 mm, ±125.0 mm and ±150.0 mm, in order to provide indications of the horizontal variation of the wall temperature. The ambient air temperature was measured by the same type of thermocouples located in the proximity of the leading edge of the channel. Fifteen thermocouples were affixed to the rear surface of the plates and embedded in the polystyrene block, in order to evaluate the conductive heat losses. Thermocouple voltages were recorded to 1 μV. Each thermocouple was calibrated in a 0.01 K thermostatic bath using a reference standard thermometer (Pt 100). The calibration of the temperature measuring system showed an estimated precision of the thermocouple-readout system of ±0.2 K. A National Instruments SCXI module data acquisition system and a personal computer were

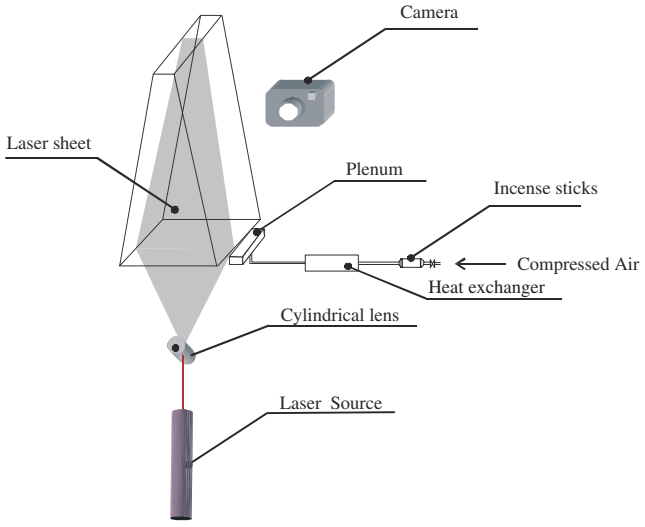

Fig. 2. Flow visualization equipment.

used for the data collection and reduction. The data acquisition was performed through the LabView™ software.

Tests showed the wall temperature to be symmetric between the two heated plates at the same x location, the differences being within ± 0.2 °C. Wall temperature was assumed to be independent of y coordinate within ± 100 mm, since its maximum deviation from the centerline temperature was found to be no greater than 1.2 °C when the latter was 80.0 °C.

Smoke for visualization was generated by burning incense sticks in a steel tube, connected to a compressor (Fig. 2). The smoke was injected through a glass heat exchanger to reduce the temperature of the smoke. The smoke passed into a plenum and its temperature was controlled using a thermocouple. This value was close to that of the incoming ambient air into the channel. Then it was driven in the test section through a small slot situated along the leading edge of the channel. The visualization was made possible by means of a laser sheet, generated by a He–Ne laser source. The laser sheet was produced by placing a mirror near the end of the test section at an angle of 45° with respect to the direction of the main flow, after which a cylindrical lens was placed to enlarge the beam as needed. A fine regulation was allowed by means of a micrometer screw system, in order to obtain photos at the $y = 0$ plane.

3. Data reduction

The channel Rayleigh number and the modified channel Rayleigh number are defined as:

$$Ra = Gr\,Pr = \frac{g\beta q_c b^4}{\nu^2 k} Pr \text{ and } Ra' = Ra\frac{b}{L} \tag{1}$$

where q_c is the spatially-averaged convective heat flux

$$q_c = \frac{1}{L}\int_0^L q_c(x)\,dx \tag{2}$$

In the following step reference will be made to three different Rayleigh numbers, based on the characteristic length b_{min}, b_{max} and $b_{av} = (b_{max} + b_{min})/2$, with the aim of finding the correlation which more accurately merges the convergent channel results with those for the parallel-walled channel.

Nusselt numbers will be based on the difference between the wall and the inlet fluid temperatures, rather than on that between the wall and the bulk fluid temperatures, since the latter cannot be easily measured in practical applications. The channel Nusselt number is defined as

$$Nu = \frac{q_c b}{(T_w - T_o)k} \tag{3}$$

where T_w is the average wall temperature

$$T_w = \frac{1}{L}\int_0^L T_w(x)\,dx \tag{4}$$

The dimensionless temperature is defined as

$$T^+ = \frac{T - T_o}{\frac{q_c b}{k}} \tag{5}$$

Also for Nusselt numbers, reference will be made to b_{min}, b_{max} and b_{av}.

The properties of the air are evaluated at the reference temperature $(T_w + T_o)/2$.

Local convective heat flux, $q_c(x)$, is not uniform because of radiation and conduction. Experimental data are reduced first by introducing, in the equations presented above, the local heat flux

$$q_c(x) = q_\Omega(x) - q_k(x) - q_r(x) \tag{6}$$

In Eq. (6), the overall heat rate divided by the area of the wall surface is the local heat flux due to Ohmic dissipation, $q_\Omega(x)$, which was assumed to be uniform along the heated plates; $q_k(x)$ denotes the local conduction heat losses from the plates and $q_r(x)$ is the local radiative heat flux from the plates. For each run, the terms $q_k(x)$ were calculated by a finite difference numerical procedure, assuming a two-dimensional distribution of the temperature in the polystyrene. The predicted temperatures in significant configurations of the system had been previously compared to those measured by the thermocouples embedded in the polystyrene insulation and the agreement was very good, the maximum deviation being $\pm 4\%$. The $q_r(x)$ terms were calculated for each temperature distribution in the walls, ambient temperature and channel spacing, dividing each plate into 10 equal length strips along the channel, according to the procedure described by Webb and Hill [17]. For all the investigated configurations the conductive heat losses were about 9% of the Ohmic wall heat flux, whereas the radiative heat losses ranged between about 3% and 5%.

The uncertainty in the calculated quantities was determined according to the standard single sample analysis recommended in [18]. The uncertainty of a dependent variable R as a function of the uncertainties in the independent variables X_i is given by the relation

$$\delta R = \left[\left(\frac{\partial R}{\partial X_1} \delta X_1 \right)^2 + \left(\frac{\partial R}{\partial X_2} \delta X_2 \right)^2 + \cdots + \left(\frac{\partial R}{\partial X_n} \delta X_n \right)^2 \right]^{1/2} \tag{7}$$

The uncertainty in the values of the air thermophysical properties were assumed to be negligible. The maximum percentage uncertainties in the values of the independent variables were: 0.5% for T_w, 0.93% for T_o, 1.1% for $(T_w–T_o)$, 1.2% for b_{min}, 2.0% for q_Ω, 4.0% for q_k, 3.0% for q_r and 5.0% for q_c. On the basis of Eqs. (1), (3), (5) the maximum uncertainty in Ra'_{bmin} was 6.7% whereas the maximum uncertainty in Nu_{bmin} turned out to be 3.4%.

4. Mathematical model and numerical procedure

The numerical model presented in [9] allows the solution of the physical domain shown in Fig. 3a. It consists of two non-parallel plates which form a convergent channel. Both plates are conductive and heated at uniform heat flux q_Ω. The flow in the channel is assumed to be two-dimensional, laminar, incompressible, with negligible viscous dissipation. The working fluid is air ($Pr = 0.71$) and all thermophysical properties of the fluid are assumed to be constant, except for the dependence of density on the temperature (Boussinesq approximation) which gives rise to the buoyancy forces. The thermophysical properties of the fluid are evaluated at the ambient temperature, T_o, which is assumed to be 300 K in all cases.

The governing equations, for the fluid region in steady state regime, are

$$\frac{\partial u}{\partial x} + \frac{\partial v}{\partial y} = 0 \tag{8}$$

$$u\frac{\partial u}{\partial x} + v\frac{\partial u}{\partial y} = -\frac{1}{\rho_f}\frac{\partial p}{\partial x} + \nu\left(\frac{\partial^2 u}{\partial x^2} + \frac{\partial^2 u}{\partial y^2}\right) - g\beta(T - T_o) \tag{9}$$

$$u\frac{\partial v}{\partial x} + v\frac{\partial v}{\partial y} = -\frac{1}{\rho_f}\frac{\partial p}{\partial y} + \nu\left(\frac{\partial^2 v}{\partial x^2} + \frac{\partial^2 v}{\partial y^2}\right) \tag{10}$$

$$u\frac{\partial T}{\partial x} + v\frac{\partial T}{\partial y} = a_f\left(\frac{\partial^2 T}{\partial x^2} + \frac{\partial^2 T}{\partial y^2}\right) \tag{11}$$

A two-dimensional conduction model in the walls is employed; radiative heat transfer is neglected. The heat transfer equation in the steady state regime with constant thermophysical properties is

$$\frac{\partial^2 T_s}{\partial x^2} + \frac{\partial^2 T_s}{\partial y^2} = 0 \tag{12}$$

Since the two plates are placed in an infinite medium, the problem has been solved by taking a computational domain of finite extent, as depicted in Fig. 3b, and by following the approach given in [19]. The upstream and downstream reservoirs have been employed to simulate the free-stream condition of the flow away from the region of the thermal disturbance induced by the heated plates. The imposed boundary conditions for the fluid and solid domains are reported in Table 2. The pressure defect equals zero on the inlet and outlet boundaries.

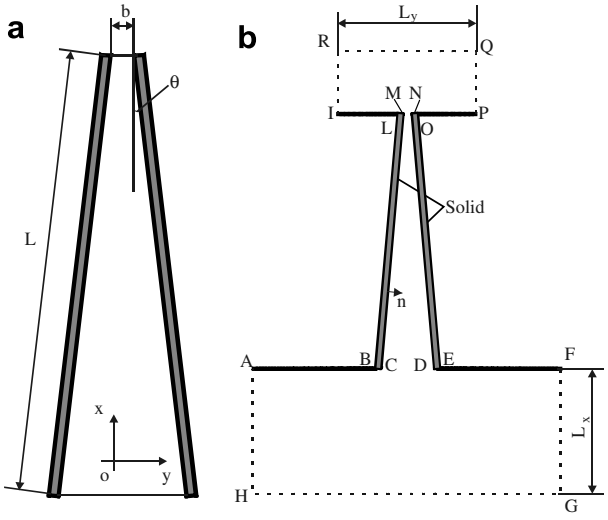

Fig. 3. Sketch of the configuration (a) and computational domain (b).

Table 2
Boundary conditions for the domain

Wall	u	v	T
Fluid domain			
AH and FG	$\frac{\partial u}{\partial y} = 0$	$\frac{\partial v}{\partial y} = 0$	$T = T_o$
HG	$\frac{\partial u}{\partial x} = 0$	$\frac{\partial v}{\partial x} = 0$	$T = T_o$
AB, EF, IL, OP	$u = 0$	$v = 0$	$\frac{\partial T}{\partial x} = 0$
BC, DE, LM, NO	$u = 0$	$v = 0$	$k_f\frac{\partial T}{\partial x} = k_s\frac{\partial T}{\partial x}$
DN	$u = 0$	$v = 0$	$k_f\frac{\partial T}{\partial n} = k_s\frac{\partial T}{\partial n} + q_\Omega$
CM	$u = 0$	$v = 0$	$k_f\frac{\partial T}{\partial n} = k_s\frac{\partial T}{\partial n} - q_\Omega$
RQ	$\frac{\partial u}{\partial x} = 0$	$\frac{\partial v}{\partial x} = 0$	$\frac{\partial T}{\partial x} = 0$ if $u > 0$; $T = T_o$ if $u < 0$
IR	$\frac{\partial u}{\partial y} = 0$	$\frac{\partial v}{\partial y} = 0$	$\frac{\partial T}{\partial y} = 0$ if $v < 0$; $T = T_o$ if $v > 0$
QP	$\frac{\partial u}{\partial y} = 0$	$\frac{\partial v}{\partial y} = 0$	$\frac{\partial T}{\partial y} = 0$ if $v > 0$; $T = T_o$ if $v < 0$
Solid domain			
DN			$k_f\frac{\partial T}{\partial n} = k_s\frac{\partial T}{\partial n} + q_\Omega$ and $T_s = T_f$
CM			$k_f\frac{\partial T}{\partial n} = k_s\frac{\partial T}{\partial n} - q_\Omega$ and $T_s = T_f$
BL, OE			$\frac{\partial T}{\partial n} = 0$
BC, DE, LM, NO			$k_f\frac{\partial T}{\partial x} = k_s\frac{\partial T}{\partial x}$ and $T_s = T_f$

A finite volume method was employed to solve Eqs. (8)–(12) and the commercial code Fluent [20] was used to carry out numerical results. Several preliminary tests were carried out with different methods of solution. Since results were nearly equal for the same conditions, the quicker method was employed. The segregated solution method was chosen to solve the governing equations, which were linearized implicitly with respect to the equation's dependent variable. The first-order upwind scheme was chosen for the unsteady energy and momentum equations. The semi implicit method for pressure-linked equations (SIMPLE) scheme was chosen to couple pressure and velocity. Computation starts with zero values for the velocity components and with pressure and temperature values equal

to the ambient values. The convergence criteria were 10^{-5} for the residuals of the velocity components and 10^{-6} for the residuals of the energy equation.

Preliminary results were obtained to evaluate the effect of the grid. The configuration examined was the case with $b_{\min} = 32.3$ mm, $\theta = 10^{\circ}$ at $q_{\Omega} = 120$ W/m^2. The average Nusselt numbers were evaluated for different grids, with the following number of nodes in the channel: 50×100, 100×200, 150×300, 80×400, 100×400 and 200×400. Differences between Nusselt numbers for the 100×400 and 200×400 were nearly 4% and the former was chosen in order to obtain the results.

As to the dimensions of the reservoirs, $L_x = L$ and $L_y = 10 b_{\min}$ were chosen, since they do not affect the velocity and temperature in the channel, as it was reported in [19]. A more detailed description of the numerical model and procedure is given in [9,10].

5. Results

Experiments were carried out in air ($Pr = 0.71$) for $b_{\min} = 7.0$–40.0 mm, $\theta = 0^{\circ}$, 2°, 5° and 10° and $q_{\Omega} = 30$, 60, 120 and 220 W/m^2, corresponding to a Ra'_{bmin} from 2.85 to 1.22×10^5.

5.1. Wall temperatures

Wall temperature profiles as a functions of the axial coordinate are reported in Figs. 4–6 for the investigated values of spacing, of the convergence angle θ and heat flux q_{Ω}.

For $b_{\min} = 7.0$ mm and $q_{\Omega} = 30$ W/m^2, Fig. 4a, at the exit section the percentage decrease of wall temperature value with respect to the maximum wall temperature is about 16% for $\theta = 0^{\circ}$ whereas it is between 17% and 20% for $\theta \geqslant 2^{\circ}$. When the value of the heat flux increases, Fig. 4b and c, the percentage decrease becomes higher. For convergence angles $\theta \geqslant 2^{\circ}$, wall temperature values are higher than the ones for $\theta = 0^{\circ}$ in the lower part of the heated wall because in this zone the velocity is lower, even in boundary layer, due to a larger transversal section. In a convergent channel the boundary layers adjacent the walls interact at a lower x value than the one for $\theta = 0^{\circ}$. Furthermore, for each convergence angle θ when the heat flux value increases, the value of the coordinate x, where the interaction between the boundary layers is attained, is higher. In fact, when the value of the heat flux, hence the Rayleigh number, increases, the boundary layer becomes thinner. For $\theta \geqslant 2^{\circ}$ temperatures are lower than the ones for $\theta = 0^{\circ}$ at the higher part of the channel walls because fluid velocity adjacent the walls increases. Discrepancies between maximum wall temperature in the range 2–10° are lower than the ones between 0° and 2°.

When the value of $b_{\min} = 10.0$ mm, Fig. 5, maximum temperature values are lower than the ones for $b_{\min} = 7.0$ mm for each value of heat flux and convergence angle. In particular, the decrement is equal to 8% for $q_{\Omega} = 30$ W/m^2 and $\theta = 0^{\circ}$ and 18% for $q_{\Omega} = 120$ W/m^2 and $\theta = 0^{\circ}$. Furthermore, percentage differences between maximum temperature values for $\theta = 0^{\circ}$ and $\theta \geqslant 2^{\circ}$ are lower than the ones for $b_{\min} = 7.0$ mm. In fact, the percentage difference is 11% for $q_{\Omega} = 30$ W/m^2, 15% for $q_{\Omega} = 60$ W/m^2, 9% for $q_{\Omega} = 120$ W/m^2, 4% for $q_{\Omega} = 220$ W/m^2. For $b_{\min} = 10.0$ mm the boundary layer is thinner than the one for $b_{\min} = 7.0$ mm because Rayleigh number is higher. Therefore, the point, where the temperature profiles for $\theta = 0^{\circ}$ and $\theta \geqslant 2^{\circ}$ intersect, is closer to the channel exit section and lies in the channel upper half.

For $b_{\min} = 20.0$ mm, Fig. 6, differences between maximum temperature values for investigated convergence

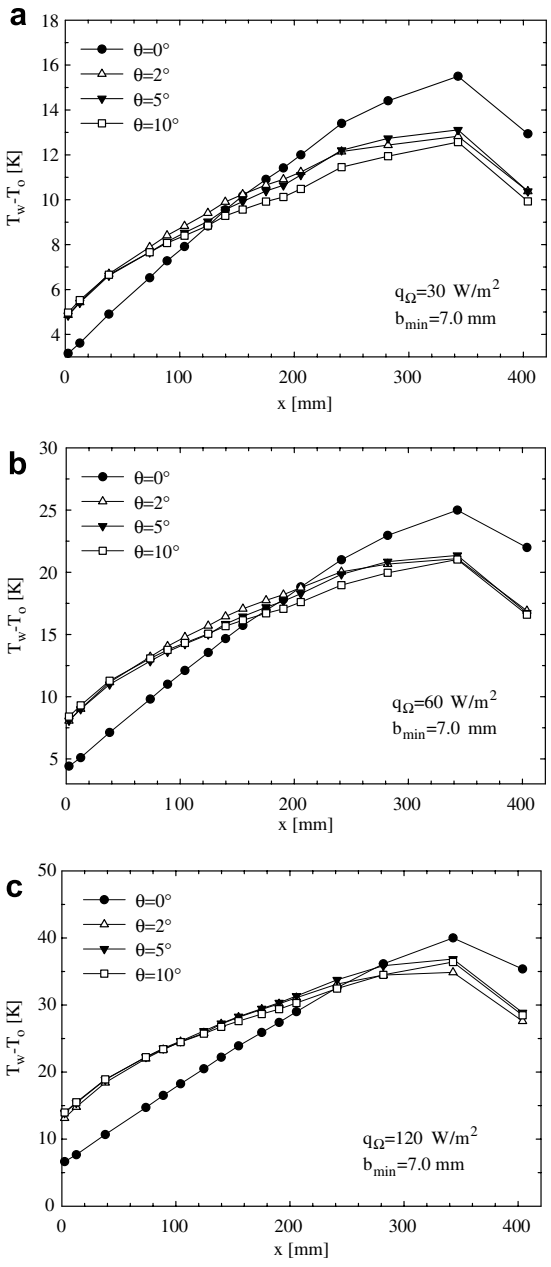

Fig. 4. Wall temperature rise above the ambient temperature vs. the vertical coordinate, for $b_{\min} = 7.0$ mm and $\theta = 0$, 2, 5, 10°: (a) $q_{\Omega} = 30$ W/m^2; (b) $q_{\Omega} = 60$ W/m^2; (c) $q_{\Omega} = 120$ W/m^2.

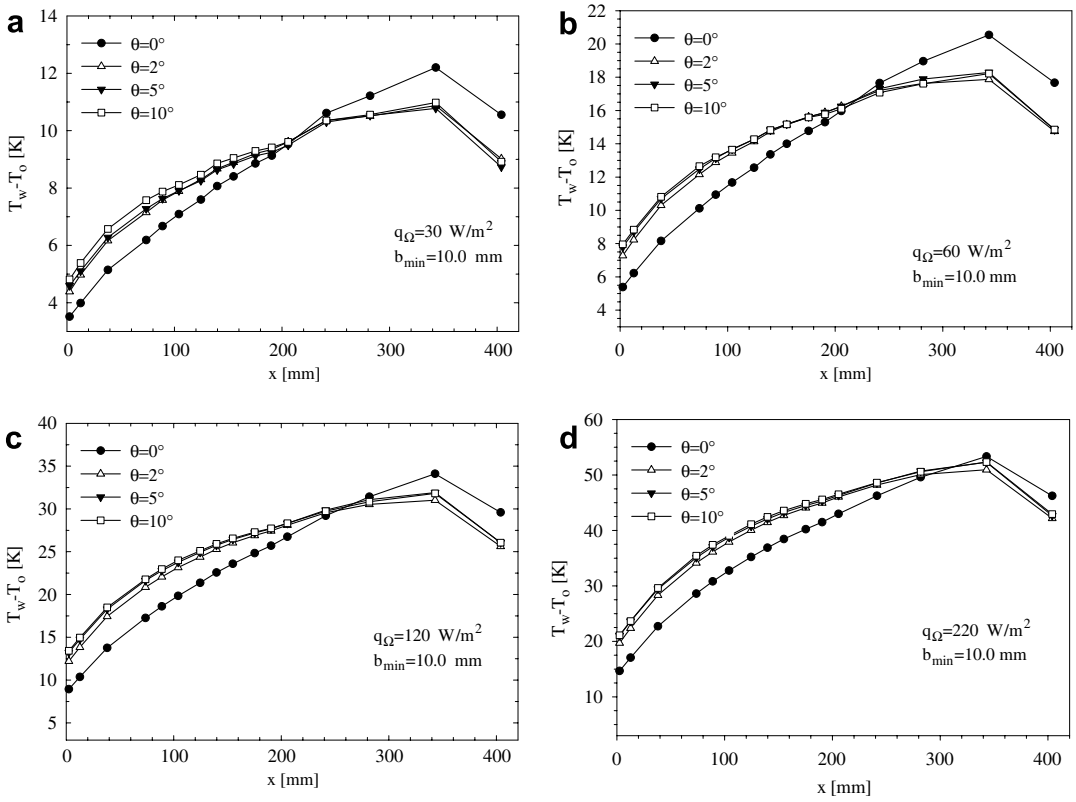

Fig. 5. Wall temperature rise above the ambient temperature vs. the vertical coordinate, for $b_{min} = 10.0$ mm and $\theta = 0, 2, 5, 10°$: (a) $q_\Omega = 30$ W/m^2; (b) $q_\Omega = 60$ W/m^2; (c) $q_\Omega = 120$ W/m^2; (d) $q_\Omega = 220$ W/m^2.

angles are lower than the ones for $b_{min} = 10.0$ mm, maximum percentage difference being equal to 3% between $\theta = 0°$ and 2° for $q_\Omega = 60$ W/m^2. This suggests that for b_{min} values greater than 20.0 mm, a convergent channel is not recommended in order to contain wall maximum temperature. A significant advantage in the use of a convergent channel is for low b_{min} values and convergence angle almost 2°. This is in accordance with numerical results reported in [8–10] and theoretical analysis given in [13].

Fig. 7 shows maximum wall temperature, referred to the ambient temperature, as a function of b_{min} for the investigated convergence angles and for several heat flux values. This figure allows for a detection of optimal thermal configurations with respect to maximum wall temperature for converging channels. For each heat flux value, the changes of maximum wall temperature with convergence angle decrease when b_{min} increases and this discrepancy is higher than 2 K for b_{min} values up to about 10 mm. In each case, the worst configuration for $b_{min} \leqslant 10$ mm is the one with parallel heated walls. For b_{min} higher than 10 mm maximum wall temperature are attained at $\theta < 10°$. When b_{min} increases, the values of the maximum wall temperature diminish, but the percentage drop passing from $b_{min} = 20.0$ mm to $b_{min} = 40.0$ mm is much lower than percentage drop passing from $b_{min} = 7.0$ mm to $b_{min} = 20.0$ mm. This suggests that high b_{min} values are not favourable for the thermal control. In order to reduce maximum wall temperature values, high b_{min} values are not advantageous because they imply an increase of system volume without a significant decrease of maximum wall temperature, according to [8,21,22]. For low b_{min} values, optimal convergence angle is at $\theta = 2°$ whereas when b_{min} increases, optimal angle is at about $\theta = 0°$. However, maximum wall temperature values attained for $\theta = 2°$ are close to the lower ones. In either case, the best configuration regarding the volume is $\theta = 2°$.

5.2. Correlations for dimensionless maximum wall temperature and average Nusselt number

Maximum wall temperatures reported in the previous figure are made dimensionless by Eq. (5) where the reference length is b_{min}, b_{max} or b_{av}. Correlations between dimensionless maximum wall temperature and channel Rayleigh number can be obtained by means of least square method. The correlations have the following expression

$$T_b^+ = \alpha (Ra'_b)^\beta \tag{13}$$

The values of the coefficient α and β are reported in Table 3 as functions of the reference lengths b_{min}, b_{max} and b_{av}. Experimental data and the corresponding correlations are reported in Fig. 8. A better correlation was obtained with $Ra_{bmax}\left(\frac{b_{min}}{b_{max}}\right)^{2/5}$ as the independent variable, as suggested in [13]. The corresponding expression is

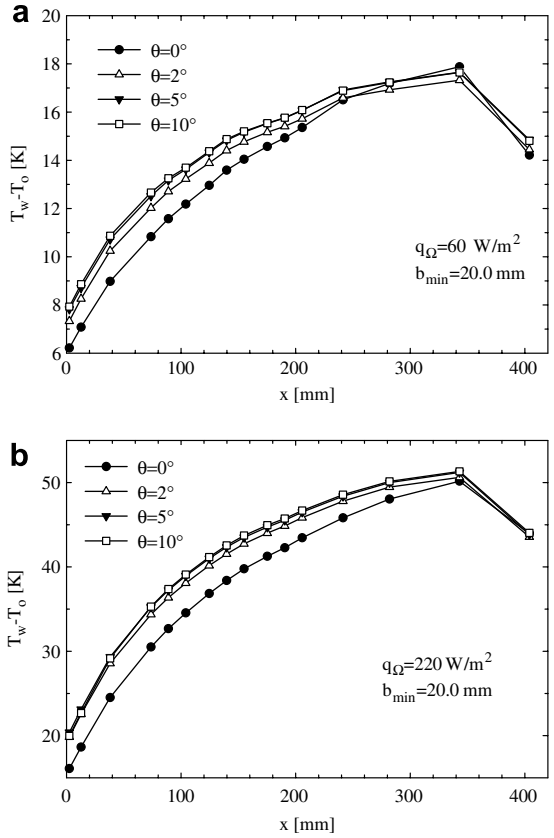

Fig. 6. Wall temperature rise above the ambient temperature vs. the vertical coordinate, for $b_{min} = 20.0$ mm and $\theta = 0$, 2, 5, 10°: (a) $q_\Omega = 60$ W/m^2; (b) $q_\Omega = 220$ W/m^2.

$$T^{+}_{max,bmax} = 8.50\left[Ra_{bmax}\left(\frac{b_{min}}{b_{max}}\right)^{2/5}\right]^{-0.27} \quad (14)$$

with $r^2 = 0.995$ and valid for $196 < Ra_{bmax} < 4.89 \times 10^8$ and $4.73 \times 10^{-2} < \frac{b_{min}}{b_{max}} < 1$ ranges. This correlation allows to evaluate the dimensionless maximum wall temperature when the emissivity, ε, of the channel walls is 0, whereas the correlation proposed in [13] is valid for $\varepsilon > 0$.

Fig. 9 shows the good agreement between the correlation of Eq. (14) and the experimental data.

As proposed in [3], the channel Nusselt number and the channel Rayleigh number, $Ra' = Ra(b/L)$, were referred to the three characteristic lengths b_{min}, b_{av} and b_{max} and correlated in the following form

$$Nu_b = nRa'^{m}_b \quad (15)$$

The coefficients in Eq. (5) were obtained by means of the least square method and are reported in Table 4, together with the regression coefficients. It is worth noticing that the worst correlation ($r^2 = 0.983$) was obtained by basing the Nusselt and Rayleigh numbers on the average spacing. Channel Nusselt and modified Rayleigh numbers, based on b_{min}, b_{av} and b_{max}, as well as the regression curves are reported in Fig. 10a–c. The correlations are in the following range: $2.85 \leqslant Ra'_{bmin} \leqslant 1.22 \times 10^5$ and $0° \leqslant \theta \leqslant 10°$.

Channel Nusselt number and channel Rayleigh number were also correlated by the following monomial equation

$$Nu_b = nRa^{m}_b \quad (16)$$

whose coefficients, for b_{min}, b_{av} and b_{max}, are reported in Table 3. Experimental data as well as the regression curves, based on b_{min}, b_{av} and b_{max}, are reported in Fig. 11a–c, respectively. The best correlation of experimental data were obtained by adopting b_{max} as a characteristic length. The regression coefficients at any spacing values are larger than those in Table 4. However, it is worth remarking that the coefficients in Eq. (15) are very similar to those for the single plate. One can conclude that the thermal performance of a convergent channel with a maximum spacing b_{max} is, for practical purposes, equal to that of a parallel-walled channel with a spacing $b = b_{max}$.

5.3. Flow visualization and numerical stream function and temperature fields

In the following, a comparison between experimental and numerical data are accomplished in terms of experimental flow visualization and numerical stream function fields. The comparison is given in Figs. 12–14 for convergence angles equal to 2°, 5°, and 10°, for $b_{min} = 7.0$, 20.0 and 32.3 mm and for $q_\Omega = 30$ and 120 W/m^2.

Pictures of the flow patterns in the channel and stream function fields for a convergence angle equal to 2° and a ohmic heat flux equal to 120 W/m^2 are reported in Fig. 12 for $b_{min} = 7.0$ mm (a, b) and 20.0 mm (c, d). Both numerical and experimental results show a laminar boundary layer near the channel walls. At the channel inlet, the boundary layers do not interact both for $b_{min} = 7.0$ mm and 20.0 mm. It is observed, but not shown here, that for the parallel walled channel, the interaction between the two boundary layers starts in the zone near the channel inlet.

For a convergence angle equal to 5°, pictures of the flow patterns and stream function fields for $q_\Omega = 30$ and 120 W/m^2 are reported in Fig. 13 for $b_{min} = 7.0$ mm (Fig. 13a, b, e, f) and 20.0 mm (Fig. 13c, d, g, h). For $b_{min} = 7.0$ mm, both numerical and experimental results show a recirculating zone in the central part of the channel. This is due to the two symmetric boundary layers that merge in the exit region of the channel and the convergence angle as well. The velocity component along y is not zero and tends toward the centerline of the channel. These two effects choke the channel flow and generate the recirculating region. By comparing Fig. 13a and b, related to $q_\Omega = 30$ W/m^2, with Fig. 13e and f, related to $q_\Omega = 120$ W/m^2, it is observed that the recirculating zone moves up when the ohmic heat flux increases. This effect can be explained with the decrease of the boundary layer thickness. The recirculating zone is not present for $b_{min} = 20.0$ mm, even if a separation of the streamlines in the central part of the channel is detected for $q_\Omega = 120$ W/m^2, Fig. 13h. These figures show a good agreement between numerical and experimental results, also in accordance with [9,10,12].

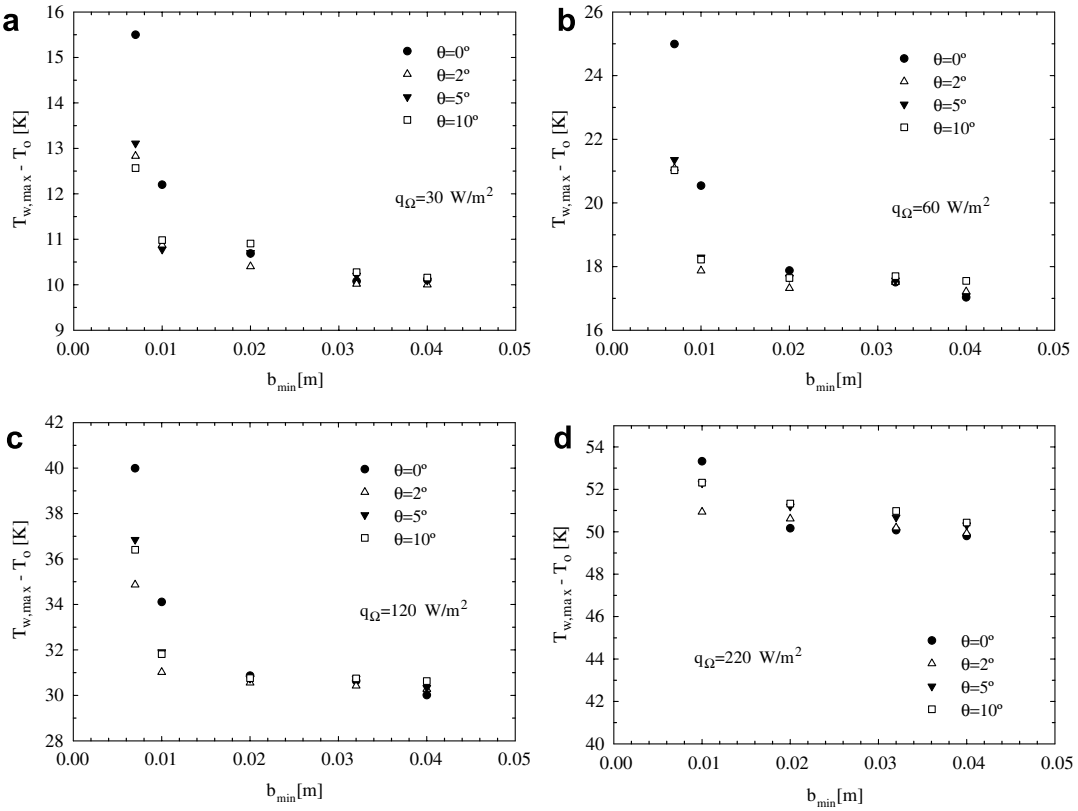

Fig. 7. Maximum wall temperature rise above the ambient temperature as a function of b_{min}, for $\theta = 0$, 2, 5, 10°: (a) $q_\Omega = 30$ W/m^2; (b) $q_\Omega = 60$ W/m^2; (c) $q_\Omega = 120$ W/m^2; (d) $q_\Omega = 220$ W/m^2.

Table 3
Coefficients in Eqs. (13) and (16)

	$T_b^+ = \alpha(Ra'_b)^\beta$; Eq. (13)			$Nu_b = n\,Ra_b^m$; Eq. (16)		
	α	β	r^2	n	m	r^2
$b = b_{min}$	2.80	−0.22	0.988	0.15	0.26	0.991
$b = b_{av}$	2.49	−0.20	0.978	0.20	0.24	0.989
$b = b_{max}$	2.39	−0.20	0.985	0.20	0.24	0.994

In Fig. 14, pictures of the flow patterns and stream function fields for a convergence angle equal to 10°, for $q_\Omega = 30$ and 120 W/m^2 are reported. In this case, for $q_\Omega = 30$ W/m^2 results for $b_{min} = 7.0$ mm and 20.0 mm are reported (Fig. 14a–d), whereas for $q_\Omega = 120$ W/m^2, results are related to $b_{min} = 7.0$ mm and 32.3 mm (Fig. 14e–h). These figures show that for $\theta = 10°$ and for $b_{min} = 7.0$ mm, the recirculating zones are larger and situated at a larger x than for $\theta = 5°$. In fact, in this case, due to the larger convergence angle, the boundary layers meet at a larger x coordinate and the vortexes move up when the heat flux increases. Fig. 14c and d show that for this convergence angle ($\theta = 10°$), a recirculating zone is also present for $b_{min} = 20.0$ mm. In this case, this zone is closer to the outlet of the channel than the corresponding case with $b_{min} = 7.0$ mm. It was observed, but not shown here, that the channel is also chocked for $b_{min} = 20.0$ mm and $q_\Omega = 120$ W/m^2. For this heat flux value, flow patterns for $b_{min} = 32.3$ mm are reported to show that, for this minimum channel spacing value, the channel is not chocked and no recirculating zones are present. Here the boundary layers do not interact, as shown in Fig. 14h. Also in this case the figures show a very good agreement between experimental and numerical results.

In Fig. 15, numerically obtained temperature fields for $\theta = 5°$, $q_\Omega = 30$ W/m^2 and 120 W/m^2 are reported for $b_{min} = 7.0$ mm (Fig. 15a and c) and 20.0 mm (Fig. 15b and d). The thermal boundary layer thickness decreases with the ohmic heat flux; in fact the isotherm related to the ambient temperature penetrates more inside the channel for $q_\Omega = 120$ W/m^2 than for $q_\Omega = 30$ W/m^2. This effect is more pronounced for $b_{min} = 20.0$ mm than for $b_{min} = 7.0$ mm. For $b_{min} = 7.0$ mm, a maximum relative temperature on the centerline is observed in the central part of the channel. This is clearly due to the recirculating zone that moves hot air downward from the upper zones. This

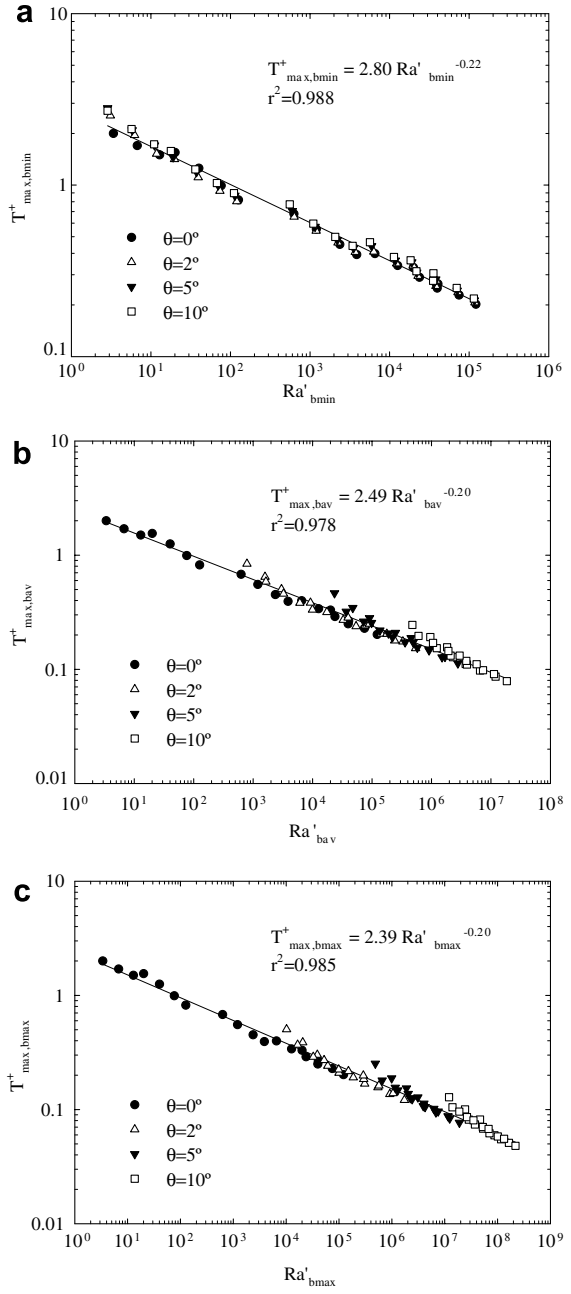

Fig. 8. Dimensionless maximum wall temperature rise above the ambient temperature vs. the modified Rayleigh number: (a) $b = b_{min}$; (b) $b = b_{av}$; (c) $b = b_{max}$.

effect is not detectable for $b_{min} = 20.0$ mm; in this case the vortexes are not present as shown in Fig. 13.

Numerically obtained temperature fields for $\theta = 10°$, $q_\Omega = 30\ W/m^2$ and $120\ W/m^2$ are reported in Fig. 16. Here, for $q_\Omega = 30\ W/m^2$, results for $b_{min} = 7.0$ mm and 20.0 mm are reported (Fig. 16a and b), whereas for $q_\Omega = 120\ W/m^2$, results are related to $b_{min} = 7.0$ mm and 32.3 mm (Fig. 16c and d). By comparing Fig. 16a–c, with Fig. 15a–c, it is observed that the distance from the inlet at which the thermal field can be considered fully developed does not depend on the convergence angle, for the

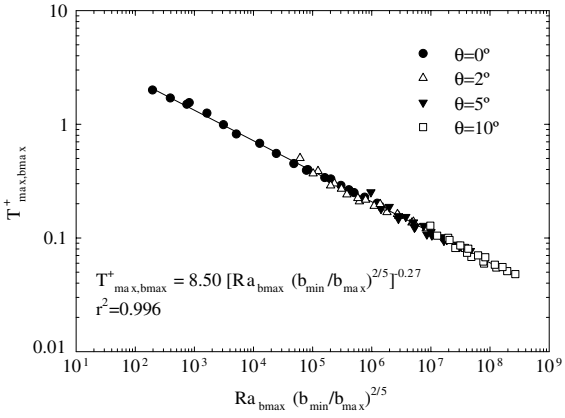

Fig. 9. Dimensionless maximum wall temperature rise above the ambient temperature vs. $Ra_{bmax}(b_{min}/b_{max})^{0.4}$.

Table 4
Coefficients in Eq. (15)

	$b = b_{min}$	$b = b_{av}$	$b = b_{max}$
n	0.48	0.57	0.59
m	0.21	0.19	0.19
r^2	0.987	0.983	0.989

two considered θ values. Isotherms in Fig. 16b ($\theta = 10°$, $q_\Omega = 30\ W/m^2$, $b_{min} = 20.0$ mm) show the presence of the recirculating zone detected by the flow patterns presented in Fig. 14c and d. For $b_{min} = 32.3$ mm, Fig. 16d, the ambient isotherm penetrates inside the channel, very close to the channel exit and the thermal boundary layers meet only at almost the exit of the channel. In this case, isotherms show that no recirculating zones are present.

6. Conclusions

An experimental investigation on natural convection in air ($Pr = 0.71$) in a convergent channel with symmetric heating was accomplished, in order to analyze the effects of the channel spacing, convergence angle and heat flux. The channel walls were heated at uniform heat flux. Results in terms of wall temperature profiles as a function of the walls inclination angle, the channel spacing and the heat flux were given. Nusselt numbers and dimensionless maximum temperatures were evaluated and correlated to the modified Rayleigh number based on minimum value of spacing between the plate, b_{min}, in the $2.85–1.22 \times 10^5$ range and $0° \leqslant \theta \leqslant 10°$.

For the lowest spacing value, the parallel plate configuration, $\theta = 0°$, presented the highest maximum wall temperature and for a small increase of the convergence angle, $\theta = 2°$, a remarkable decrease was noticed. For $\theta > 2°$, maximum wall temperature presented a slight decrease. These results confirmed the numerical analysis given in [8–10]. Moreover, for larger channel spacings, $b_{min} \geqslant 20$ mm, wall temperatures increased at increasing

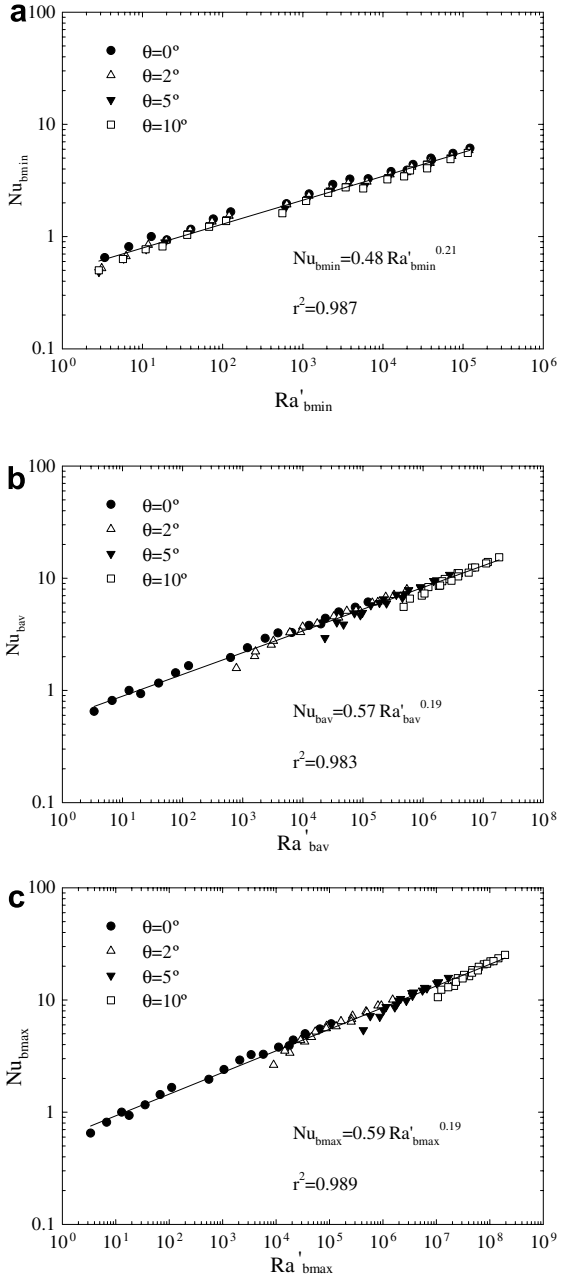

Fig. 10. Channel Nusselt number vs. the modified Rayleigh number: (a) $b = b_{min}$; (b) $b = b_{av}$; (c) $b = b_{max}$.

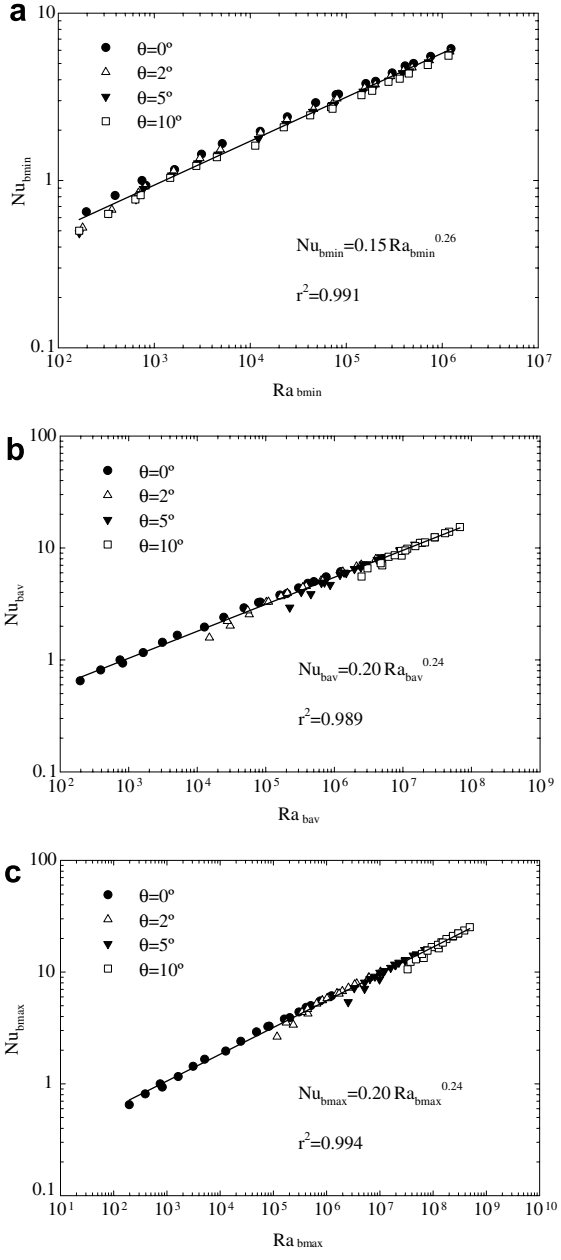

Fig. 11. Channel Nusselt number vs. the Rayleigh number: (a) $b = b_{min}$; (b) $b = b_{av}$; (c) $b = b_{max}$.

converging angles at any spacings, whereas they were almost independent of the spacing at larger values of the heat flux. However, it is worth remarking that the dependence of wall temperature on the inclination angle was smaller in the exit region of the channel.

Dimensionless maximum wall temperatures and average Nusselt numbers were correlated with channel Rayleigh numbers in monomial equations. It was found that, for the dimensionless maximum wall temperatures, the best monomial correlation in terms of *Ra*' was obtained with b_{min} as reference length and a very good correlation was carried out in terms of $Ra_{bmax}\left(\frac{b_{min}}{b_{max}}\right)^{2/5}$. It is suitable for emissivity of the channel walls, $\varepsilon = 0$ and, together with the correlation proposed in [13], completes the ε range to evaluate maximum wall temperatures. The best correlation for the Nusselt number was obtained in terms of channel Rayleigh number with b_{max} as reference length. The correlations were evaluated in the ranges: $195 \leqslant Ra_{bmax} \leqslant 4.89\times 10^8$ and $0^\circ \leqslant \theta \leqslant 10^\circ$.

A comparison between experimental flow visualization and stream function fields obtained numerically was accomplished and a good agreement was observed. Numerical and experimental results showed a recirculating zone in the central part of the channel for convergence angles greater than 5° and for several minimum channel spacing

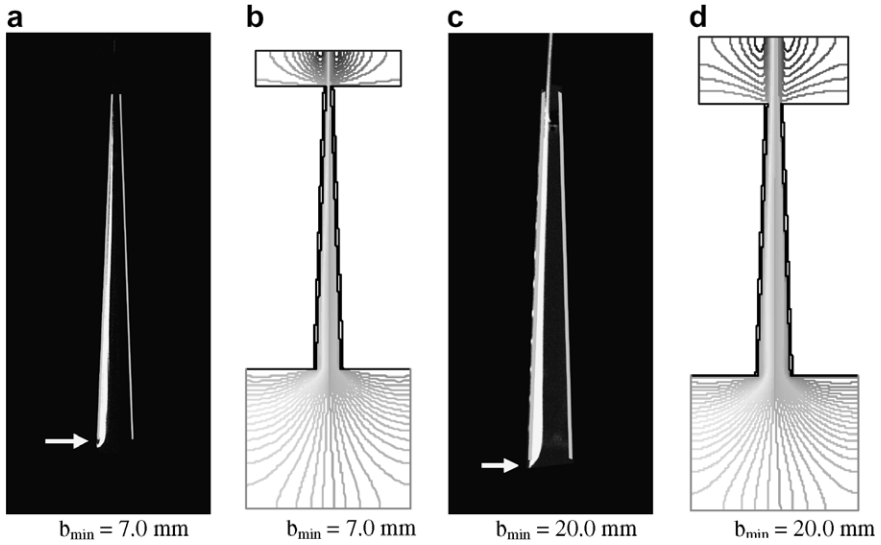

Fig. 12. Flow pattern pictures and stream function fields for $q_\Omega = 120\ \mathrm{W/m^2}$, $\theta = 2^\circ$, and for several b_{min} values.

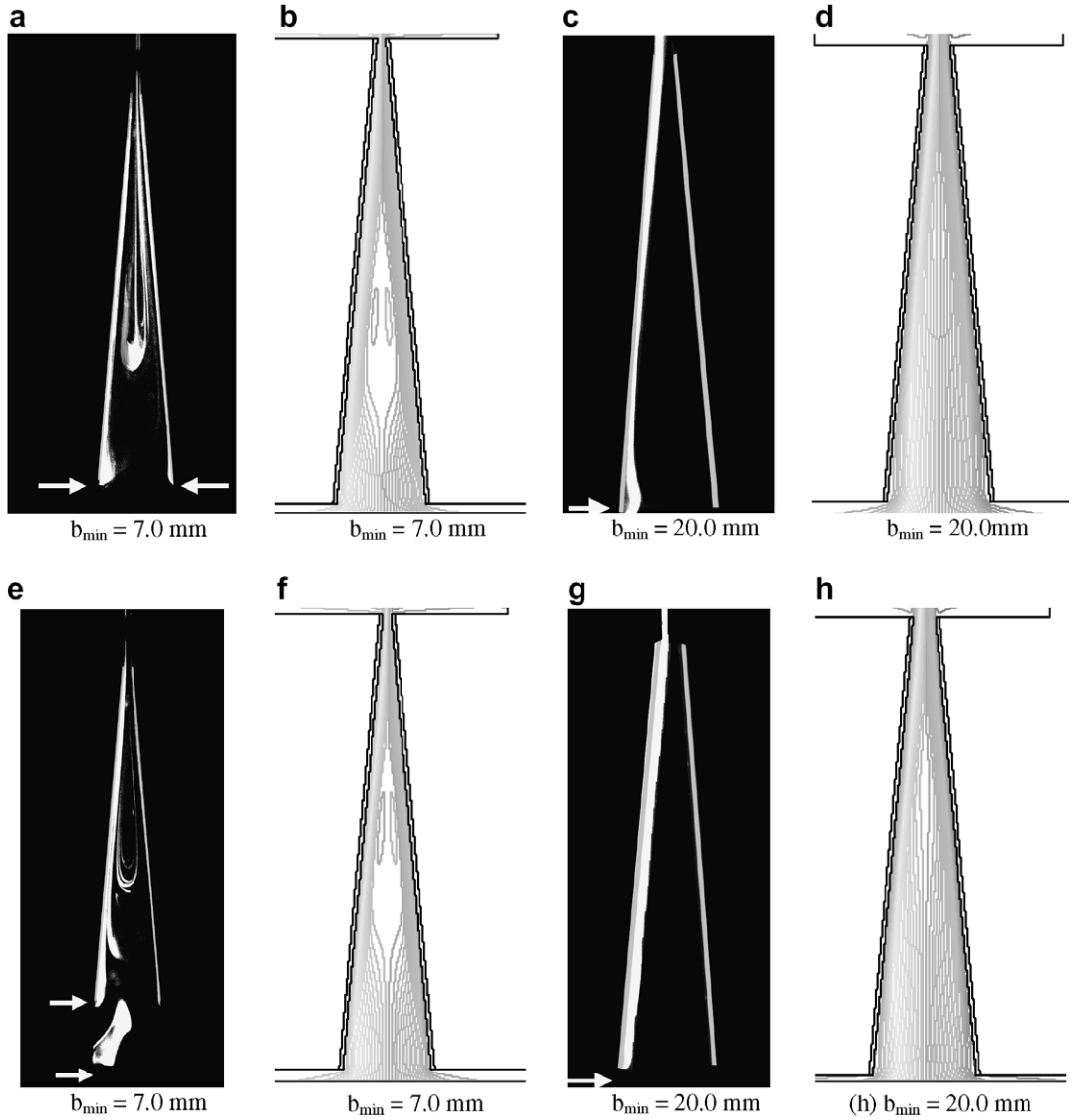

Fig. 13. Flow pattern pictures and stream function fields for $\theta = 5^\circ$ and for several q_Ω and b_{min} values: (a–d) $q_\Omega = 30\ \mathrm{W/m^2}$; (e–h) $q_\Omega = 120\ \mathrm{W/m^2}$.

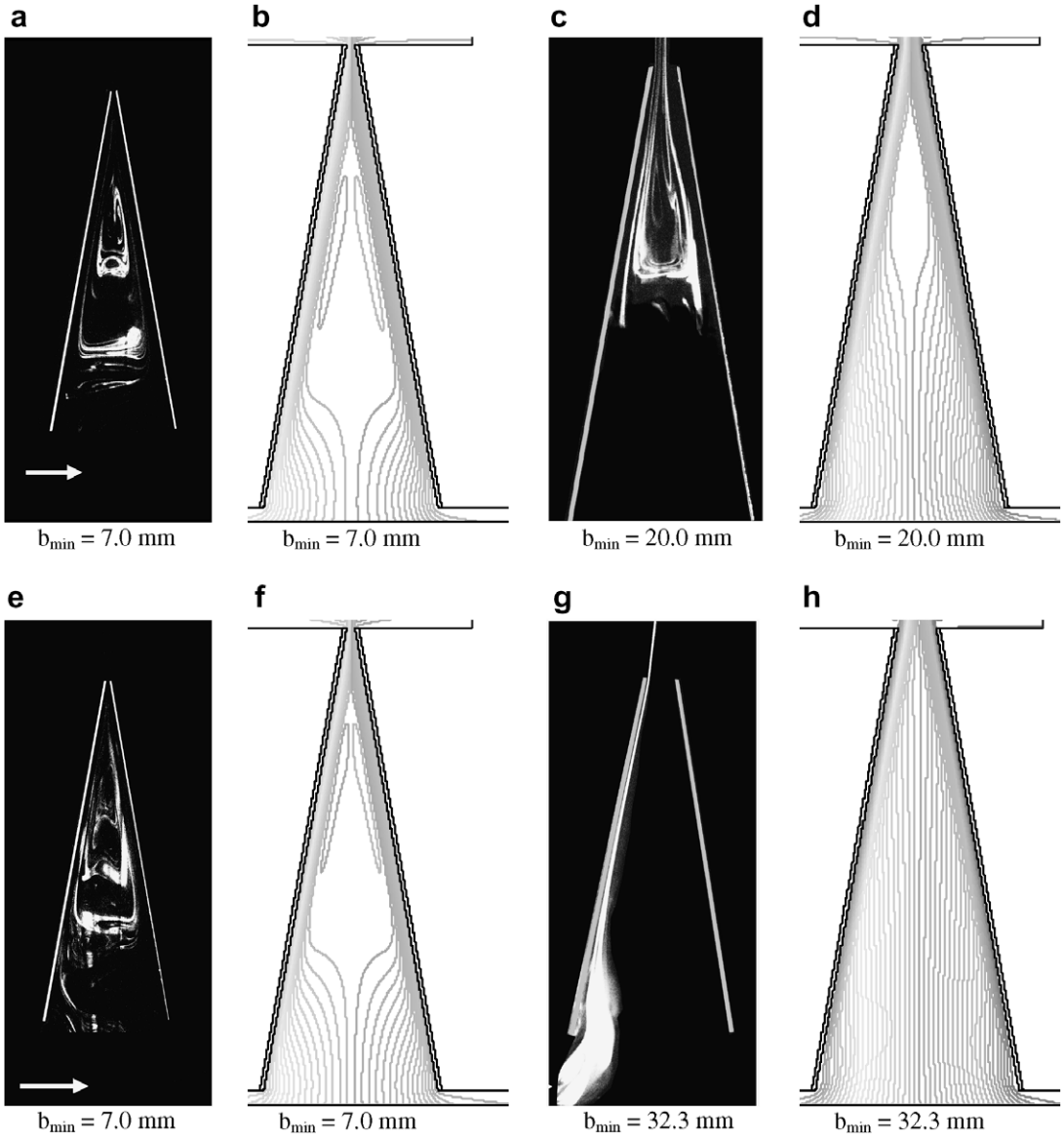

Fig. 14. Flow pattern pictures and stream function fields for $\theta = 10^\circ$ and for several q_Ω and b_{min} values: (a–d) $q_\Omega = 30\ W/m^2$; (e–h) $q_\Omega = 120\ W/m^2$.

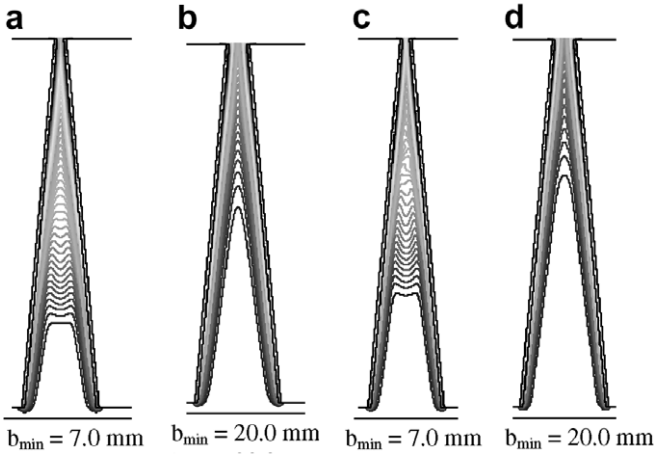

Fig. 15. Temperature fields for $\theta = 5^\circ$ and for several q_Ω and b_{min} values: (a, b) $q_\Omega = 30\ W/m^2$; (c, d) $q_\Omega = 120\ W/m^2$.

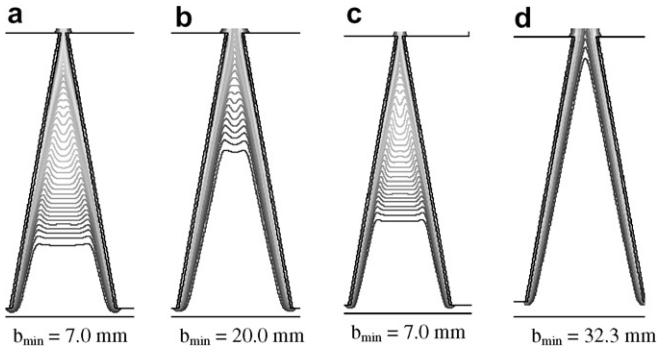

Fig. 16. Temperature fields for $\theta = 10^\circ$ and for several q_Ω and b_{min} values: (a, b) $q_\Omega = 30\ W/m^2$; (c, d) $q_\Omega = 120\ W/m^2$.

values according with [9,10,12]. These values increased with the convergence angle. The vortexes moved up when the heat flux or the convergence angle increased. The distance from the inlet at which the temperature fields could be considered fully developed increased with the ohmic heat flux, but it did not depend on the convergence angle for the two considered values. The recirculating zone induced a relative maximum of the temperature on the channel centerline.

Acknowledgements

This research is supported by Seconda Università degli Studi di Napoli and by Ministero dell'Istruzione dell'Università e della Ricerca with the 2005 PRIN Grant research program.

References

[1] G.P. Peterson, A. Ortega, Thermal control of electronic equipment cooling, in: J.P. Hartnet, T.F. Irvine (Eds.), Advances in Heat Transfer, Academic Press, New York, 1990, pp. 181–314.
[2] O. Manca, B. Morrone, S. Nardini, V. Naso, Natural convection in open channels, in: B. Sundén, G. Comini (Eds.), Computational Analysis of Convection Heat Transfer, WIT Press, Southampton, 2000, pp. 235–278.
[3] E.M. Sparrow, R. Ruiz, L.F.A. Azevedo, Experimental and numerical investigation of natural convection in convergent vertical channels, Int. J. Heat Mass Transfer 31 (1988) 907–915.
[4] E.M. Sparrow, R. Ruiz, Experiments on natural convection in divergent vertical channels and correlation of divergent, convergent, and parallel-channel Nusselt numbers, Int. J. Heat Mass Transfer 31 (1988) 2197–2205.
[5] S.A. Said, Investigation of natural convection in convergent vertical channels, Int. J. Energy Res. 20 (1996) 559–567.
[6] J.S. Shalash, J.D. Tarasuk, D. Naylor, Experimental and numerical studies of natural convection heat transfer in vertical converging channel flows, in: M. Giot, F. Mayinger, G.P. Celata (Eds.) Proceedings of Fourth Experimental Heat Transfer, Fluid Mechanics and Thermodynamics, Brussels, 1997, pp. 2167–2174.
[7] A.S. Kaiser, B. Zamora, A. Viedma, Correlations for Nusselt number in natural convection in vertical converging channels at uniform temperature by numerical investigation, Int. J. Heat Fluid Flow 25 (2004) 671–682.
[8] A. Bejan, A.K. da Silva, S. Lorente, Maximal heat transfer density in vertical morphing channels with natural convection, Numer. Heat Transfer – Part A 45 (2004) 135–152.
[9] N. Bianco, S. Nardini, Numerical Analysis of natural convection in air in a vertical convergent channel with uniformly heated conductive walls, Int. Commun. Heat Mass Transfer 32 (2005) 758–769.
[10] N. Bianco, L. Langellotto, O. Manca, V. Naso, Numerical analysis of radiative effects on natural convection in vertical convergent and symmetrically heated channels, Numer. Heat Transfer – Part A 49 (2006) 369–391.
[11] T.M. Huang, C. Gau, W. Aung, Mixed convection flow and heat transfer in a heated vertical convergent channel, Int. J. Heat Mass Transfer 38 (1995) 2445–2456.
[12] F. Marcondes, V. de Souza Melo, J.M. Gurgel, Numerical analysis of natural convection in parallel, convergent, and divergent open-ended channels, Int. J. Numer. Meth. Heat Fluid Flow 16 (3) (2006) 304–323.
[13] N. Bianco, L. Langellotto, O. Manca, S. Nardini, Thermal design and optimization of vertical convergent channels in natural convection, Appl. Therm. Eng. 26 (2006) 170–177.
[14] N. Bianco, B. Morrone, S. Nardini, V. Naso, Air Natural Convection between Inclined Parallel Plates with Uniform Heat Flux at the Walls, Int. J. Heat Technol. 18 (2000) 23–46.
[15] G.A. Ledezma, A. Bejan, Optimal geometric arrangement of staggered vertical plates in natural convection, ASME J. Heat Transfer 119 (1997) 700–708.
[16] K.D. Kihm, J.H. Kim, L. Fletcher, Investigation of natural convection heat transfer in vertical converging channel flows using a specklegram technique, ASME J. Heat Transfer 115 (1993) 140–148.
[17] B.W. Webb, D.P. Hill, High Rayleigh number laminar natural convection in an asymmetrical heated vertical channel, ASME J. Heat Transfer 111 (1989) 649–656.
[18] R.J. Moffat, Describing the uncertainties in experimental results, Exp. Therm. Fluid Sci. 1 (1988) 3–17.
[19] Andreozzi, O. Manca, Thermal and fluid dynamic behaviour of symmetrically heated vertical channels with auxiliary plate, Int. J. Heat Fluid Flow 22 (2001) 424–432.
[20] Fluent Incorporated, Fluent 6.1, User Manual, 2003.
[21] A. Bejan, Shape and Structure from Engineering to Nature, Cambridge University Press, New York (NY), 2000.
[22] A.K. da Silva, A. Bejan, Constructal multi-scale structure for maximal heat transfer density in natural convection, Int. J. Heat Fluid Flow 26 (2005) 34–44.